ADVANCED MATERIALS INTERFACES
www.advmatinterfaces.de

The $Pb(Zr_{0.2},Ti_{0.8})O_3$/ZnO/GaN Ferroelectric–Semiconductor Heterostructure: Insight into the Interfacial Energy Level Alignments

*Juan Wang, Regan G. Wilks, Roberto Félix, Xia X. Liao, Alexei Grigoriev, and Marcus Bär**

Ferroelectric/semiconductor heterostructures promise to be the backbone of next-generation "green" data storage devices combining ultrashort switching times and ultralow switching power with a simplified device structure and low-cost processing. One promising candidate to realize such resistive memory devices is the ferroelectric-$Pb(Zr_{0.2},Ti_{0.8})O_3$/semiconductor–ZnO/GaN heterostructure. A detailed knowledge about the energy level alignments in this heterostructure is of utmost importance to understand the charge carrier transport mechanism as that is what determines the macroscopic performance of corresponding ferroelectric/semiconductor-based electronic devices. Employing hard X-ray photoelectron spectroscopy, favorable type-II energy level alignments at the $Pb(Zr_{0.2},Ti_{0.8})O_3$/ZnO and ZnO/GaN interfaces are found with, however, significantly lower offsets in the valence as well as the conduction band for the latter. As a result, the formation of a high-resistance state and a low-resistance state can be explained by a combination of polarization effects and related changes in the energy level alignment. The charge carrier transport through the $Pb(Zr_{0.2},Ti_{0.8})O_3$/ZnO/GaN heterostructure may in the low-resistance state be limited by the significant hole barrier at the ZnO/GaN interface. The gained insight opens a new route for device optimization by deliberate interface engineering promising improved tunable resistive memory devices.

1. Introduction

Ferroelectric/semiconductor heterostructures have drawn increasing attention due to their promising applications in electronics.[1–3] An aggressive prospect is to utilize the switchable polarization of ferroelectrics to control the charge distribution in the semiconductor layer by inducing an electric field at the ferroelectric/semiconductor interface.[4] This opens the route for large-scale use of ferroelectric materials in energy conversion applications, e.g., in solar water splitting, photovoltaic, and solar fuel devices.[5] Moreover, ferroelectric/semiconductor field-effect transistors (FETs) have been proposed, with the potential to exceed the performance of existing FET technology for non-volatile memory applications.[6] Especially the combination of ultrashort switching times and ultralow switching power with a simplified device structure and low-cost processing make ferroelectric/semiconductor heterostructures the prime candidate to be used in next-generation "green" data storage devices.

Zinc oxide (ZnO) is an attractive semiconductor candidate material for forming

Dr. J. Wang, Dr. R. G. Wilks, Dr. R. Félix, Dr. X. X. Liao, Prof. M. Bär
Interface Design
Helmholtz-Zentrum Berlin für Materialien und Energie GmbH (HZB)
Berlin 12489, Germany
E-mail: marcus.baer@helmholtz-berlin.de
Dr. J. Wang, Prof. A. Grigoriev
Department of Physics and Engineering Physics
The University of Tulsa
Tulsa, OK 74104, USA
The ORCID identification number(s) for the author(s) of this article can be found under https://doi.org/10.1002/admi.202000201.

DOI: 10.1002/admi.202000201

Dr. R. G. Wilks, Prof. M. Bär
Energy Materials In-Situ Laboratory Berlin (EMIL)
Helmholtz-Zentrum Berlin für Materialien und Energie GmbH
Berlin 12489, Germany
Dr. X. X. Liao
School of Material Science and Engineering
Nanchang University
Nanchang 330031, P. R. China
Prof. M. Bär
Helmholtz-Institute Erlangen-Nürnberg for Renewable Energy (HI ERN)
Berlin 12489, Germany
Prof. M. Bär
Department of Chemistry and Pharmacy
Friedrich-Alexander-Universität Erlangen-Nürnberg
Erlangen 91054, Germany

ferroelectric/semiconductor heterostructures, due to its excellent material compatibility with ferroelectrics,[7,8] such as $Pb(Zr,Ti)O_3$ (PZT). High-quality PZT/ZnO heterostructures can be fabricated without using a buffer layer, and its application in memory devices has been investigated.[9] In addition, due to its direct wide bandgap ($E_g^{ZnO} = 3.37$ eV),[10] ZnO is a candidate material employed in short-wavelength light-emitting devices (LED), especially in GaN-based LEDs because of their same wurtzite crystal structure, small lattice mismatch of 1.9%, and similar energy bandgap ($E_g^{GaN} = 3.40$ eV).[11]

To understand the electronic properties of PZT/ZnO/GaN heterostructures, it is crucial to have detailed insight into the energy level alignment at the PZT/ZnO/GaN interfaces. Energy level alignments of the involved interfaces have previously been constructed using published electron affinity and work function values, and they suggest the presence of, e.g., a valence band offset (VBO) of 0.48 eV and a conduction band offset (CBO) of 0.85 eV[12,13] at the PZT/ZnO interface and a VBO of 0.6 eV at the ZnO/GaN heterostructure.[14] However, directly measured energy level alignment data for ZnO/GaN and/or PZT/ZnO heterointerfaces are scarce. For the ZnO/GaN heterostructure, a VBO of ≈1.0 eV,[15] derived by ultraviolet and X-ray photoelectron spectroscopy measurements, has been reported. The significant deviation of this measured value from that suggested based on reported electron affinities and work functions (0.6 eV, see above) highlights the importance of experimentally derived insights into the energy level alignment at the PZT/ZnO/GaN interfaces.

To close this knowledge gap, we report on directly measured shallow core level (CL), and valence band maximum (VBM) derived density of states (DOS) of ZnO/GaN and PZT/ZnO/GaN heterointerfaces as probed by hard X-ray photoelectron spectroscopy (HAXPES). The corresponding energy level alignments are derived and discussed. This information is expected to be used to explain and predict the charge carrier transport in PZT/ZnO/GaN-based electronic devices, which will ultimately guide further deliberate optimization efforts.

2. Results and Discussion

First, we focus on the determination and discussion of the VBM position with respect to the Fermi level (E_F) of the GaN substrate and the 40 nm thick ZnO/GaN sample. The corresponding HAXPES spectra of the shallow CL region show all expected lines, e.g., O 2s, Ga 3d, and Zn 3d (see **Figure 1**a). The VBM positions were estimated by linear approximation of the leading edges of the spectral onset to the respective baselines, as shown in Figure 1b. The selection of data points used in the linear fit of the leading edge has a potential effect on the obtained VBM value. We chose several different sets of points over the linear region of the leading edge for linear approximation and found the uncertainty of VBM related to the choice of data points was less than 0.05 eV for GaN and 0.03 eV for ZnO in the present work. Together with the uncertainty of the energy calibration of the electron analyzer and beamline, we estimate the total error to be in the order of ±0.10 eV in both cases. As displayed in Figure 1b, the VBM of the GaN substrate was determined to be (−3.30 ± 0.10) eV, agreeing with previously reported values ranging from 2.7 to 3.5 eV.[14,16,17] The proximity

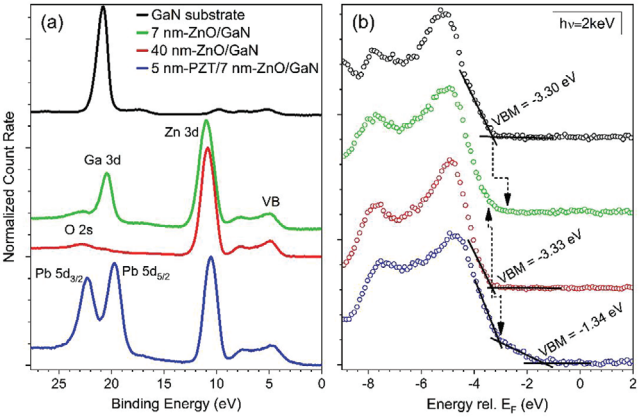

Figure 1. a) 2 keV excited HAXPES spectra of the valence band (VB) and shallow core level (O 2s, Ga 3d, Pb 5d, and Zn 3d) region of the GaN substrate, the 7 and 40 nm thick ZnO films on GaN, and the 5 nm PZT/7 nm ZnO/GaN layer stack. b) Magnified (renormalized) view of the valence band maximum (VBM) regions from (a). The linear approximation of the leading spectral edges and the correspondingly derived VBM values (±0.10 eV) are indicated. For the 7 nm ZnO/GaN layer stack, the expected VBM positions of GaN and ZnO are indicated by the arrows using the VBM values of the GaN and 40 nm ZnO/GaN sample and considering interface induced band bending derived from the shift of the shallow core levels (Zn 3d and Ga 3d; see Table S1 in the Supporting Information). For the 5 nm PZT/7 nm ZnO/GaN sample, the arrow indicates the VB onset attributed to ZnO.

of the VBM value of GaN to its bandgap energy (3.40 eV[11]) implies that E_F is near the conduction band minimum (CBM). Assuming flat band conditions at the sample surface, this indicates pronounced n-type conductivity of the GaN substrate, in agreement with the doping concentration stated in the Experimental Section (i.e., 1×10^{18} cm^{-3}). The VBM of the 40 nm ZnO/GaN sample is located at (−3.33 ± 0.10) eV, which agrees well with previous reports for ZnO (3.2–3.5 eV).[18–20]

The VBM regions of the heterointerface samples (i.e., samples that have a cover layer thickness that allows probing the underlying material) are more difficult to interpret directly due to the superposition of signals from multiple layers. This is prominently demonstrated by the Ga 3d (of GaN) and Zn 3d (of ZnO) shallow CL lines in the spectra of the 7 nm ZnO/GaN and the 5 nm PZT/7 nm ZnO/GaN sample, respectively. The proximity of the n-GaN and ZnO VBM values make the direct determination of the VBM alignment from the spectrum of the 7 nm ZnO/GaN impossible; the seemingly more pronounced foot at the spectral onset will be discussed below. In contrast, the VBM of PZT is expected to be at significantly lower values; previously reported values range between 1.4 and 1.7 eV.[21,22] Close inspection of the VB onset of the 5 nm PZT/7 nm ZnO/GaN sample in Figure 1b indeed shows a significant foot, which we ascribe to the VBM of PZT. The derived VBM position is (1.34 ± 0.10) eV in agreement with the literature values mentioned above. The kink around 3 eV is attributed to the VBM of ZnO, as discussed below.

In order to account for band bending induced by the interface formation, we consult the energy shifts of the shallow CLs upon layer deposition. Note that the Ga 3d line overlaps with Pb 5d derived states for the PZT/ZnO/GaN sample, which has to be taken into consideration in the fit model. Furthermore,

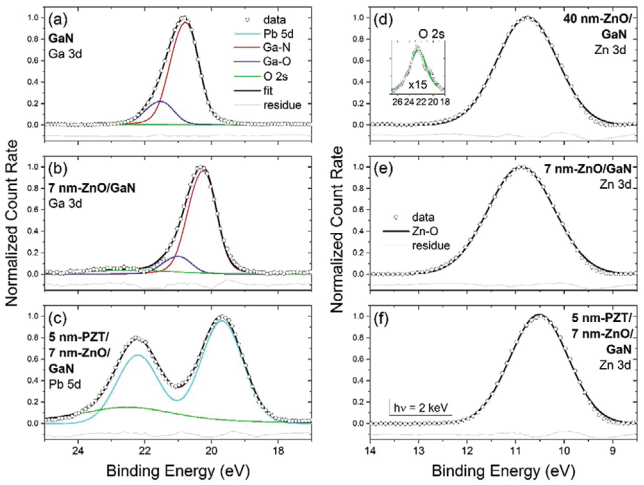

Figure 2. 2 keV excited Ga 3d and O 2s HAXPES spectra for a) the GaN substrate and b) the 7 nm ZnO/GaN sample. Pb 5d/O 2s and Zn 3d HAXPES spectra are shown in (c) for the 5 nm PZT/7 nm ZnO/GaN sample and in d) for the 40 nm ZnO/GaN, in e) for the 7 nm ZnO/GaN, and in f) for the 5 nm PZT/7 nm ZnO/GaN samples, respectively. The inset in panel (d) shows the O 2s line (with presumably some Ga 3d derived spectral remnants) on a magnified (15×) scale. Open points represent the experimental data, and solid black lines represent the total fit after (Shirley) background subtraction. For the individual fit components, Voigt (mixed Lorentzian–Gaussian) line shapes (or doublets thereof) were employed. The residua are shown as solid gray lines below the data/fit. The fitted peak positions[15,29,32–35] are summarized in Table S1 in the Supporting Information.

the shallow CLs in Figure 1, especially the Zn 3d line, are of low enough binding energy that they will have some band-like character, and we also note that their spectral width varies between samples. We, therefore, in the fitting procedure for the Zn 3d, allow the width of the Voigt peaks (see respective FWHM—full width at half-maximum—values in Table S1 in the Supporting Information) to vary while maintaining the spin–orbit splitting and branching ratio. The resulting Zn 3d energy positions therefore have a relatively larger uncertainty due to this imperfect treatment of the effects of band dispersion and of the potential for separate contributions from surface, bulk, and interface.

Figure 2 displays the HAXPES spectra of Ga 3d, Pb 5d, and Zn 3d CLs, fitted by Voigt (mixed Lorentzian–Gaussian) peaks after subtraction of Shirley backgrounds. Figure 2a–c shows the Ga 3d spectrum of the GaN substrate, the 7 and 40 nm ZnO/GaN, and the 5 nm PZT/7 nm ZnO/GaN heterojunctions. The spectra of the first two samples were fitted by three contributions, two Ga 3d lines (assigned to the bonding configurations of Ga–N, Ga–O[23,24]) and one broad O 2s line. Ga oxide often forms at the GaN surface when exposed to ambient conditions or at the ZnO/GaN interface during ZnO deposition, as Ga can diffuse from the GaN surface, bonding with oxygen.[25–27] Each Ga 3d species was fitted by two spin–orbit components (Ga $3d_{5/2}$ and $3d_{3/2}$) with an orbital splitting of 0.45 eV[28] and a branching ratio of 3:2. The binding energy shift between the Ga–N and Ga–O component was 0.75 eV for all samples.[29] The Ga 3d spectral range of the 5 nm PZT/7 nm ZnO/GaN sample is dominated by the Pb $5d_{5/2}$ and $5d_{3/2}$ doublet (spin–orbit separation: 2.52 eV, branching ratio: 3:2).[30] Furthermore, an increase in the O 2s line intensity can be observed, in agreement with the increased oxide layer thickness present on the GaN substrate and the higher relative O content in PZT compared to that in ZnO. The fits of the Zn 3d spectrum of the 7 nm and 40 nm ZnO/GaN and 5 nm PZT/7 nm ZnO/GaN heterojunctions are shown in Figure 2d–f. One superposed double-peak representing the Zn $3d_{5/2}$ and $3d_{3/2}$ contributions with a spin–orbit splitting of 0.3 eV[31] and an area ratio of 3:2 (and allowing for different FWHMs, see above) is sufficient to result in a reasonable fit. The parameters deduced from Figure 2 are summarized for clarity in Table S1 in the Supporting Information.

The VBO at the ZnO/GaN heterojunction can be calculated by using the following equation[15,36]

$$\mathrm{VBO}(\mathrm{ZnO}/\mathrm{GaN}) = (\mathrm{Ga\ 3d} - \mathrm{VBM})^{\mathrm{GaN}} - (\mathrm{Zn\ 3d} - \mathrm{VBM})^{\mathrm{ZnO}} - (\mathrm{Ga\ 3d} - \mathrm{Zn\ 3d})_{\mathrm{interface}} \quad (1)$$

Using the values in Table S1 (Supporting Information), we can compute the VBO at the ZnO/GaN interface to be (0.69 ± 0.14) eV =([20.65 − 3.30] − [10.64 − 3.33] − [20.12 − 10.77] eV). Note that we used the Ga 3d binding energy values of the Ga–N contribution for the VBO determination. The respective CBO at the ZnO/GaN interface was then estimated employing the following formula

$$\mathrm{CBO}(\mathrm{ZnO}/\mathrm{GaN}) = \mathrm{VBO} - \left(E_{\mathrm{g}}^{\mathrm{ZnO}} - E_{\mathrm{g}}^{\mathrm{GaN}}\right) \quad (2)$$

Using the room temperature bandgap for bulk ZnO and GaN (3.37 and 3.40 eV),[10,11] we estimate the CBO at the ZnO/GaN interface to be (0.72 ± 0.14) eV. The corresponding energy level alignment diagram is shown in **Figure 3**a. It reveals a type-II energy level alignment at the ZnO/GaN heterointerface, which is in agreement with ref. [10] and allows for effective charge carrier separation. The absolute energy difference between the here-derived VBO and the offset of 1.0 eV reported in ref. [10] could be explained by the GaN substrate; its doping concentration is approximately one order of magnitude lower in our case compared to ref. [10]. Because of the large offsets in the valence band and conduction band, extremely strong carrier

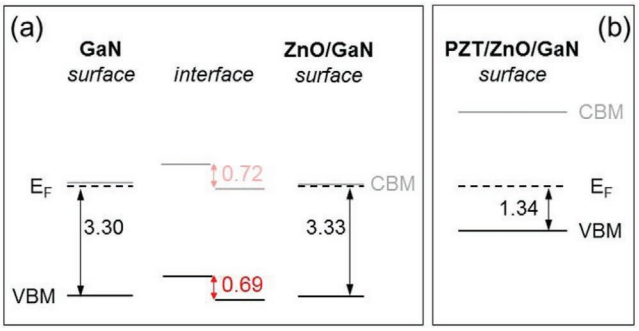

Figure 3. Schematic presentation of the energy level alignment at a) the ZnO/GaN interface and b) the position of the energy levels at the surface of the 5 nm PZT/7 nm ZnO/GaN sample as derived from HAXPES measurements (for the valence band). The position of the conduction bands are estimated (and thus shown in gray) based on Equation (2) using the bulk bandgap energy of ZnO, GaN, and $Pb(Zr,Ti)O_3$ of 3.37,[10,11] 3.40,[11] and 3.60 eV,[12] respectively.

confinement can be expected. This is very useful for unipolar electronic device applications, allowing for the realization of, e.g., high electron mobility transistors.[37]

The comparison of the position of the energy levels at the surface of the 40 nm ZnO/GaN sample in Figure 3a with that of the 5 nm PZT/7 nm ZnO/GaN sample surface in Figure 3b gives some hint of the energy level alignment at the PZT/ZnO interface and, thus, to some degree completes the alignment picture in the whole PZT/ZnO/GaN layer stack. However, note that the thickness of the ZnO varies for these samples and thus we cannot exclude that the offsets at the ZnO/GaN interface also change when considering the relevant layer stack that contains a ZnO layer of only 7 nm instead of 40 nm for which the energy level alignment of the ZnO/GaN interface was derived. Furthermore, the additional deposition of 5 nm PZT can also impact the electronic structure of the buried ZnO/GaN interface. Neglecting also any impact on the band bending due to interface formation, the VBO at the PZT/ZnO interface can be estimated to be near 2 eV. Using a bulk bandgap energy of 3.60 eV[12] for $Pb(Zr,Ti)O_3$ and employing Equation (2), this would result in a CBO in the same order of magnitude. Unfortunately, based on the available shallow CL HAXPES data, it is not possible to derive a more detailed picture of the interface induced band bending. However, the comparison of the Zn 3d line of the 40 nm ZnO/GaN with that of the 5 nm PZT/7 nm ZnO/GaN sample reveals a shift of 0.25 eV to lower binding energies (see Table S1 in the Supporting Information). Additionally, the VB onset attributed to ZnO in the spectrum of the 5 nm PZT/7 nm ZnO/GaN sample is shifted by ≈0.3 eV toward E_F compared to the VBM of the 40 nm ZnO/GaN, as indicated by the arrow in Figure 1b. This suggests an interface induced upward band bending in the ZnO toward the PZT/ZnO interface. Thus, for the 5 nm PZT/7 nm ZnO interface the VB and CB offsets of around 2 eV estimated above can be considered a higher bound limit. Directly taking the indicated ZnO VB onset in the spectrum of the 5 nm PZT/7 nm ZnO/GaN sample in Figure 1b at around 3 eV as the true VBM value, and comparing to the VBM value of the PZT gives a smaller VBO value of ≈1.7 eV. Note that this value already contains any interface-induced band bending effects. In any case, the derived VBO is much larger than the value suggested based on electron affinity values from literature (0.48 eV, see above),[12,13] emphasizing the need for a direct determination of energy level alignments.

Based on this discussion we conclude that, like the ZnO/GaN interface, the PZT/ZnO interface has a type-II energy level alignment, however, the offsets in the valence and conduction band are significantly larger. Using the reversible polarization of the ferroelectric (see schematic presentation in Figure S1 in the Supporting Information)—which can be modulated by an external electric field—it is possible to reversibly switch between a high-resistance state and a low-resistance state (see the Supporting Information for more details) as a result of the combination of polarization effects and related changes in the energy level alignment, in agreement with ref. [13]. This explains why the PZT/ZnO heterojunction is a promising candidate structure for applications in resistive memory devices. Furthermore, we find the transport barrier for holes (i.e., VBO) to be smaller than the barrier for electrons (i.e., CBO) at the PZT/ZnO interface, which is the ideal configuration for the low-resistance state as the electrical conductivity is dominated by the hole current in that case.[13] However, the charge carrier transport through the PZT/ZnO/GaN heterostructure might in this situation be limited by the significant hole barrier at the ZnO/GaN interface (see Figure 3a). Besides, the rectification ratio could benefit from an increased barrier height difference (ΔH = CBO − VBO). Thus, improved tunable resistive memory devices could be realized by deliberate interface engineering of the PZT/ZnO/GaN heterostructure.

3. Conclusion

We report for the first time the directly measured, favorable, type-II energy level alignments at the PZT/ZnO and ZnO/GaN heterointerfaces. Employing hard X-ray photoelectron spectroscopy, we find a valence band offset of (0.69 ± 0.14) eV at the ZnO/GaN interface. Considering the bulk bandgaps of ZnO and GaN, we determine the conduction band offset to be (0.72 ± 0.14) eV. For the PZT/ZnO interface, we find for both, the valence band and conduction band offset, a higher bound limit of around 2 eV. Considering the spectral onsets in the respective HAXPES spectrum of the valence band, we estimate the valence band offset to be ≈1.7 eV. Considering reversible polarization effects and related changes in the energy level alignment, high-resistance and low-resistance states can be realized at the PZT/ZnO/GaN ferroelectric/semiconductor heterostructure. In the latter case, we find that charge carrier transport might be impeded by the significant hole barrier (i.e., VBO) at the ZnO/GaN interface. This work is of utmost significance in laying the foundation for insight-driven improvements of tunable resistive memory devices.

4. Experimental Section

To study the energy level alignment at the ZnO/GaN heterointerface, undoped (but natively n-type) 7 and 40 nm thick ZnO layers (henceforth, referred to as "7 nm ZnO" and "40 nm ZnO", respectively) were deposited by 90° off-axis rf-magnetron sputtering on commercial (MTI Co.) GaN/Al_2O_3 (001) substrates ("GaN substrate"). In order to study the impact of $Pb(Zr,Ti)O_3$ (PZT) deposition on the energy level alignment at the ZnO/GaN interface, a 5 nm thick PZT layer ("5 nm PZT") was deposited by 90° off-axis rf-magnetron sputtering on a 7 nm $ZnO/GaN/Al_2O_3$ (001) heterostructure. Note that while in real-world ferroelectric applications, the PZT layer would likely be thicker; due to the high resistivity of the PZT, this study is limited to the implementation of 5 nm thick PZT layers. However, even for PZT layers down to a thickness of 4 nm stable ferroelectric polarization has been reported,[38] warranting relevance of the results of this paper. The commercial GaN/Al_2O_3 (001) substrate consists of a 4000 nm thick GaN layer with Ga polarity and n-type conductivity with typical carrier concentrations of 1×10^{18} cm^{-3}. Before film deposition, the GaN substrates were cleaned by immersing in acetone and ethanol for 1 min and 30 s, respectively, in an ultrasonic bath. To produce highly crystallized thin films, ZnO and PZT layers were fabricated at temperatures of 500 and 550 °C, respectively, while maintaining the base pressure of the vacuum system at 1×10^{-8} Torr. To obtain a material deposition rate of ≈1 nm min^{-1}, the ZnO layers were prepared under 10 mTorr partial pressure of pure Ar_2 gas flow employing 30 W sputtering power. The PZT layer was prepared (on ZnO/GaN) using a partial pressure of 30 mTorr of Ar/O_2 mixture (2:1) gas flow employing 150 W sputtering power.

The prepared GaN substrate, 7 nm ZnO/GaN, 40 nm ZnO/GaN, and 5 nm PZT/7 nm ZnO/GaN samples were studied by HAXPES using the HiKE endstation,[39] located at the BESSY II KMC-1 beamline[40] at Helmholtz-Zentrum Berlin für Materialien und Energie GmbH (HZB), using a photon energy of 2 keV. The photoelectrons were analyzed using a hemispherical analyzer (VG Scienta R4000). The Au $4f_{7/2}$ line of a clean Au foil was set to 84.00 eV to calibrate the binding energy scale. The measurements focus on probing the shallow core levels (Ga 3d, Pb 5d, O 2s, and Zn 3d) together with the valence band region to ensure a similar probing depth, simplifying data evaluation.

Supporting Information

Supporting Information is available from the Wiley Online Library or from the author.

Acknowledgements

J.W. acknowledges financial support by the DAAD RISE Professional program. R.G.W., R.F., X.X.L., and M.B. acknowledge financial support by the Impuls-und Vernetzungsfond of the Helmholtz-Association (VH-NG-423). The authors thank HZB for the allocation of synchrotron radiation beamtime.

Conflict of Interest

The authors declare no conflict of interest.

Keywords

energy level alignment, ferroelectric/semiconductor interfaces, resistive memory devices

Received: February 6, 2020
Revised: March 31, 2020
Published online: May 5, 2020

[1] V. M. Voora, T. Hofmann, M. Brandt, M. Lorenz, M. Grundmann, N. Ashkenov, H. Schmidt, N. Ianno, M. Schubert, *Phys. Rev. B* **2010**, *81*, 195307.
[2] P. W. Blom, R. M. Wolf, J. F. Cillessen, M. P. Krijn, *Phys. Rev. Lett.* **1994**, *73*, 2107.
[3] T.-L. Ren, T.-Q. Shao, W.-Q. Zhang, C.-X. Li, J.-S. Liu, L.-T. Liu, J. Zhu, Z.-J. Li, *Microelectron. Eng.* **2003**, *66*, 554.
[4] V. M. Voora, T. Hofmann, M. Schubert, M. Brandt, M. Lorenz, M. Grundmann, N. Ashkenov, M. Schubert, *Appl. Phys. Lett.* **2009**, *94*, 142904.
[5] L. Yang, Y. Xiong, W. Guo, M. Zhou, K. Song, P. Xiao, G. Cao, *Nano Energy* **2018**, *44*, 63.
[6] M. Si, A. K. Saha, S. Gao, G. Qiu, J. Qin, Y. Duan, J. Jian, C. Niu, H. Wang, W. Wu, S. K. Gupta, P. D. Ye, *Nat. Electron.* **2019**, *2*, 580.
[7] X. S. Wang, Y. J. Wang, J. Yin, Z. G. Liu, *Scr. Mater.* **2002**, *46*, 783.
[8] J. Wang, R. Leng, P. Salev, M. Cole, A. Grigoriev, *J. Appl. Phys.* **2018**, *124*, 164107.
[9] E. Cagin, D. Y. Chen, J. J. Siddiqui, J. D. Phillips, *J. Phys. D: Appl. Phys.* **2007**, *40*, 2430.
[10] D. M. Bagnall, Y. F. Chen, Z. Zhu, T. Yao, M. Y. Shen, T. Goto, *Appl. Phys. Lett.* **1998**, *73*, 1038.
[11] Y. I. Alivov, J. E. Van Nostrand, D. C. Look, M. V. Chukichev, B. M. Ataev, *Appl. Phys. Lett.* **2003**, *83*, 2943.
[12] D. F. Pan, G. F. Bi, G. Y. Chen, H. Zhang, J. M. Liu, G. H. Wang, J. G. Wan, *Sci. Rep.* **2016**, *6*, 22948.
[13] M.-X. Zhou, Z.-W. Li, B. Chen, J.-G. Wan, J.-M. Liu, *J. Phys. D: Appl. Phys.* **2013**, *46*, 165304.
[14] M. A. L. Johnson, S. Fujita, W. H. Rowland, W. C. Hughes, J. W. Cook, J. F. Schetzina, *J. Electron. Mater.* **1996**, *25*, 855.
[15] S.-K. Hong, T. Hanada, H. Makino, Y. Chen, H.-J. Ko, T. Yao, A. Tanaka, H. Sasaki, S. Sato, *Appl. Phys. Lett.* **2001**, *78*, 3349.
[16] J. Ma, B. Garni, N. Perkins, W. L. O'Brien, T. F. Kuech, M. G. Lagally, *Appl. Phys. Lett.* **1996**, *69*, 3351.
[17] S. W. King, C. Ronning, R. F. Davis, M. C. Benjamin, R. J. Nemanich, *J. Appl. Phys.* **1998**, *84*, 2086.
[18] J. W. Liu, A. Kobayashi, S. Toyoda, H. Kamada, A. Kikuchi, J. Ohta, H. Fujioka, H. Kumigashira, M. Oshima, *Phys. Status Solidi B* **2011**, *248*, 956.
[19] M. Gabás, P. Torelli, N. T. Barrett, M. Sacchi, J. R. Ramos Barrado, *APL Mater.* **2014**, *2*, 012112.
[20] T. Nagata, S. Oh, Y. Yamashita, H. Yoshikawa, R. Hayakawa, K. Kobayashi, T. Chikyow, Y. Wakayama, *Appl. Phys. Lett.* **2012**, *101*, 173303.
[21] F. Chen, R. Schafranek, W. Wu, A. Klein, *J. Phys. D: Appl. Phys.* **2011**, *44*, 255301.
[22] F. Chen, R. Schafranek, W. Wu, A. Klein, *J. Phys. D: Appl. Phys.* **2009**, *42*, 215302.
[23] T. L. Duan, J. S. Pan, N. Wang, K. Cheng, H. Y. Yu, *Nanoscale Res. Lett.* **2017**, *12*, 499.
[24] S. M. Widstrand, K. O. Magnusson, L. S. O. Johansson, E. Moons, M. Gurnett, M. Oshima, *MRS Internet J. Nitride Semicond. Res.* **2005**, *10*, e1.
[25] J. B. You, X. W. Zhang, S. G. Zhang, J. X. Wang, Z. G. Yin, H. R. Tan, W. J. Zhang, P. K. Chu, B. Cui, A. M. Wowchak, A. M. Dabiran, P. P. Chow, *Appl. Phys. Lett.* **2010**, *96*, 201102.
[26] S. Lee, D. Y. Kim, *Mater. Sci. Eng., B* **2007**, *137*, 80.
[27] S.-H. Hwang, T.-H. Chung, B.-T. Lee, *Mater. Sci. Eng., B* **2009**, *157*, 32.
[28] V. M. Bermudez, R. Kaplan, M. A. Khan, J. N. Kuznia, *Phys. Rev. B* **1993**, *48*, 2436.
[29] R. Huang, F. Li, T. Liu, Y. Zhao, Y. Zhu, Y. Shen, X. Lu, Z. Huang, J. Liu, L. Zhang, S. Zhang, Z. Li, A. Dingsun, H. Yang, *Sci. Rep.* **2018**, *8*, 8521.
[30] B. Vogt, B. Schmiedeskamp, U. Heinzmann, *Vacuum* **1990**, *41*, 1118.
[31] W. Chen, A. Kahn, P. Soukiassian, P. S. Mangat, J. Gaines, C. Ponzoni, D. Olego, *Phys. Rev. B* **1994**, *49*, 10790.
[32] J. Yang, B. S. Eller, R. J. Nemanich, *J. Appl. Phys.* **2014**, *116*, 123702.
[33] J. Moulder, W. Stickle, P. Sobol, K. Bomben, *Handbook of X-Ray Photoelectron Spectroscopy*, Physical Electronics, Inc., Eden Prairie, MN **1995**, p. 41.
[34] Q. Li, X. Ma, H. Liu, Z. Chen, H. Chen, S. Chu, *ACS Appl. Mater. Interfaces* **2017**, *9*, 18836.
[35] D. G. Popescu, M. A. Husanu, L. Trupina Combining Caron, L. Hrib, L. Pintilie, A. Barinov, S. Lizzit, P. Lacovig, C. M. Teodorescu, *Phys. Chem. Chem. Phys.* **2015**, *17*, 509.
[36] J. R. Waldrop, R. W. Grant, *Phys. Rev. Lett.* **1979**, *43*, 1686.
[37] V. O. Özçelik, J. G. Azadani, C. Yang, S. J. Koester, T. Low, *Phys. Rev. B* **2016**, *94*, 035125.
[38] T. Tybell, C. H. Ahn, J. M. Triscone, *Appl. Phys. Lett.* **1999**, *75*, 856.
[39] M. Gorgoi, S. Svensson, F. Schaefers, G. Ohrwall, M. Mertin, P. Bressler, O. Karis, H. Siegbahn, A. Sandell, H. Rensmo, W. Doherty, C. Jung, W. Braun, W. Eberhardt, *Nucl. Instrum. Methods Phys. Res., Sect. A* **2009**, *601*, 48.
[40] F. Schaefers, M. Mertin, M. Gorgoi, *Rev. Sci. Instrum.* **2007**, *78*, 123102.